^{111}Ag utilizing the (^{3}He, pnγ) reaction: A rotational nucleus with intermediate deformation

Sadek Zeghib,* F. A. Rickey, G. S. Samudra, P. C. Simms, and Ning Wang†
Tandem Accelerator Laboratory, Purdue University, Lafayette, Indiana 47907
(Received 5 January 1987)

The structure of ^{111}Ag was studied using the ^{110}Pd(^{3}He, pnγ) ^{111}Ag reaction, which has populated an essentially complete set of low-energy states. The proton exit channel was isolated from competing reaction channels by operating γ-ray detectors in coincidence with a large-solid-angle proton detector. The experiments included γ-ray excitation functions, γ-ray angular distributions, and γ-γ coincidences. Four rotational bands have been identified. A symmetric particle-rotor model has been used to interpret these bands, and the model has identified other rotational features as well. A tentative interpretation of several nonrotational states is presented, suggesting that the mixing between rotational and nonrotational states is minimal.

I. INTRODUCTION

The nature of collective motion in transitional nuclei has been the subject of extensive investigation over the past decade or so. One approach to this puzzle has been to treat transitional nuclei as slightly deformed rotors. It has been demonstrated[1-3] that many features of transitional nuclei, particularly those in the mass-100 region, can be understood in the framework of a standard symmetric particle-plus-rotor model if the Coriolis interaction is properly treated. The attractive features of the model are that it is simple, it has been studied extensively for strongly deformed nuclei, and it successfully yields systematic predictions which are a function of the position of the Fermi surface. One serious obstacle to the acceptance of this interpretation has been that the phenomena in transitional nuclei identified as rotational are not the well known rotational bands of the strongly deformed region. The present work reports a study of ^{111}Ag, whose structure provides the missing link in the puzzle. ^{111}Ag has an intermediate deformation, and evidence will be presented for four rotational bands typical of more strongly deformed nuclei as well as for features claimed to be rotational in less deformed nuclei. It will be shown that both kinds of phenomena identify rotational motion in the same nucleus and differ only in the role of the Coriolis interaction.

Previous investigations of ^{111}Ag (Refs. 4–7) had established a suggestive starting point for its interpretation, but because of the selection rules inherent to the processes utilized the results were not sufficiently complete to allow a definitive interpretation. For a more rigorous test of model predictions an experimental technique which can populate a wider range of states is desirable. Previous reports[1,8] have shown that ^{3}He induced reactions are very useful in this regard because of the large rest mass of the ^{3}He projectile. However, the study of the ^{96}Zr(^{3}He,2nγ)^{97}Mo reaction[8] showed that the complexity of spectra obtained because of other competing reaction channels can make reliable spin assignments difficult. The present investigation of ^{111}Ag utilized a large solid angle proton detector operated in coincidence with γ ray detectors to isolate the ^{110}Pd(^{3}He,pnγ)^{111}Ag reaction from other channels. The improvement in the quality of data obtained was striking, comparable to that obtained using separated isotopes rather than natural materials for targets. The experiments have resulted in a substantial extension to the known states in ^{111}Ag.

The interpretation will show that the bulk of the states observed at low excitation energies can be simply described by a symmetric particle-plus-rotor model. The basic features can in fact be deduced directly from a Nilsson diagram,[9] although the effects of the Coriolis interaction are properly included in the actual calculation. The completeness of the reaction has allowed the observation of many non-rotational states at higher excitation energies. The decay properties of the non-rotational states provide an experimental signature which is quite different from that of the rotational states. This feature has been used to suggest the identification of states involving the coupling of an odd proton to the second 2^+ state of the core. Based on this suggestion, arguments will be presented that the mixing between rotational and non-rotational degrees of freedom is minimal.

II. EXPERIMENTAL TECHNIQUES

The measurements performed in this work included γ-ray excitation functions, angular distributions, and $\gamma-\gamma$ coincidences. The target was a foil of isotopically enriched ^{110}Pd rolled to a uniform thickness of 5.1 mg/cm^2. The composition was 97.7% ^{110}Pd with the major impurity 1.3% ^{108}Pd. The two hyper-pure Ge γ-ray detectors used in these experiments had energy resolutions of $\sim$2.0 keV at 1332 keV and efficiencies of $\sim$20%. The ^{3}He beam currents of 10 to 25 nA were supplied by the Purdue FN Tandem Van de Graaff accelerator.

The gain and zero level of the detector-electronics systems were monitored during a singles experiment using the Coulomb excitation lines from the gold beam-stop and lines from a ^{60}Co source placed near the detector. From

the use of these internal standards, the energy of a relatively intense, clean γ-ray could be measured with an accuracy of approximately 100 eV. During the coincidence experiment the energy calibration was monitored by off-line measurements using a ^{182}Ta-^{152}Eu radioactive source. There are about 65 strong lines ranging from 65 keV to 1408 keV whose energies have been determined previously to $\pm$ 0.1 keV.[10] The energy dependence of the efficiencies of the detectors was also measured with the same source, since the relative intensities of these lines have also been measured previously.[10]

On-demand beam pulsing was utilized in these measurements. Every time a γ-ray was detected the beam was deflected off the target until the γ-ray pulse had been processed. This technique reduced pileup, resulting in a 200% increase in the through-put rate of useful data and a reduction in background.

Although previous experiments have demonstrated that ^{3}He induced reactions are a useful tool for populating non-yrast states, they have also been plagued by data analysis problems due to the large number of competing reactions and the small intensities of most non-yrast transitions. In the current work we have isolated the desired (^{3}He,pn) reaction by operating the γ-ray detectors in coincidence with a large-solid-angle (66%) proton detector.[11] This technique has not only removed unwanted γ-ray peaks from the spectrum but has improved the peak-to-background ratio by a factor of $\sim$6 for transitions of interest.

A. Excitation functions

Excitation functions were measured by accumulating p-γ coincidence spectra at incident ^{3}He energies of 12, 13, 14, 15, 16, and 18 MeV. The measurement served two basic functions, selecting the appropriate beam energy for subsequent experiments, and providing spin information.

Because of the proton-gamma coincidence system, the only competing reactions of concern are the (^{3}He,pn), (^{3}He,p2n), and breakup reactions. The Q-value for the (p2n) reaction (-9.27 MeV) makes it an unlikely competitor to the (pn) reaction ($Q = -0.56$ MeV) at these energies. Some very weak (p,2n) peaks were in fact observed, but they were not a problem. The major criterion in selecting the beam energy was of optimizing the (^{3}He,pn) fusion reaction relative to the breakup reaction. If the ^{3}He projectile breaks up in the Coulomb field of the target before fusion, (p,γ) or (d,nγ) reactions can occur to produce the same final nucleus as the (^{3}He,pn) reaction. In previous studies of ^{99}Ru (Ref. 1) and ^{97}Mo (Ref. 8) we have seen that the breakup process produces extremely small nuclear orientations so that angular distributions provide little spin information. In addition the angular distribution of emitted protons appears to be very forward peaked, and a large fraction of them miss the proton detector. Both the sorting efficiency of the proton-gamma system and the nuclear orientation obtained were found to increase with incident energy, indicating an increased relative probability of the fusion channel, and an incident energy of 18 MeV was selected for subsequent measurements. A typical singles spectrum is shown in Fig. 1.

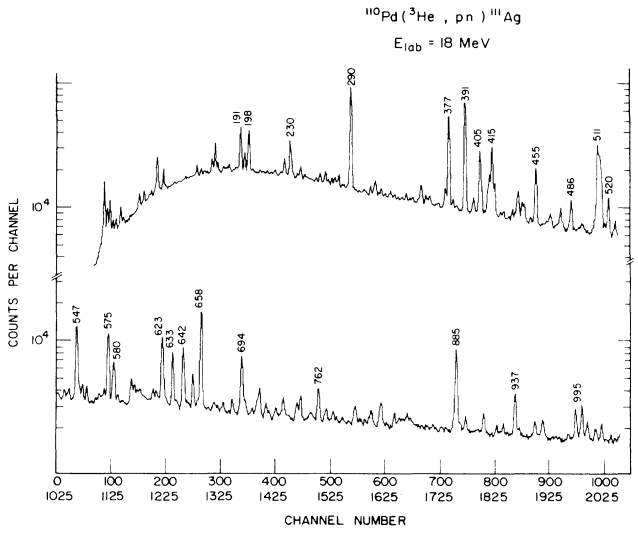

FIG. 1. Singles spectrum from the ^{110}Pd(^{3}He,pnγ) ^{111}Ag reaction.

Excitation functions also provide valuable information about the spin of the state emitting the γ ray. The dominant effect on the shape of a particular excitation function is the energy dependence of the reaction. This was removed by normalizing all excitation functions to that of the 762.12-keV transition which depopulates the $\frac{7}{2}$ state at 1153.46 keV in ^{111}Ag. It has been observed that the normalized excitation of each transition is then an exponential function of energy[12]

$$I_\gamma(E) \approx e^{bE} \quad . \tag{1}$$

As the bombarding energy increases, so does the angular momentum carried into the system. Thus the population of higher spin states increases relative to lower spin states, which is reflected in the magnitude and signs of the exponential slope b in Eq. (1). These slopes are quite characteristic of the initial spin, and can be extracted by a linear least squares fit to the logs of the normalized intensities. The use of these slopes will be discussed later.

B. Angular distributions

The angular distribution measurement consisted of proton-gated singles spectra collected at 0°, 23°, 45°, and 90° with respect to the beam axis. The alignment of the beam spot on the target with the axis of rotation of the detector was checked by placing a thin iron foil in the target position and bombarding it with 7 MeV protons. A small amount of radioactive ^{56}Co from the ^{56}Fe(p,n)^{56}Co reaction was thus produced at the beam position. Centering was then checked by counting the decay γ-radiation as a function of angle. The alignment of the zero degree point of the table with the beam axis was checked by short measurements at $+90°$ and $-90°$.

The standard angular distribution coefficients, A_{kk}, were extracted using a least squares procedure. The

theoretical angular distribution coefficients for maximum alignment, A_{kk}^0, can be readily calculated as a function of the initial spin, the change in angular momentum, and the multipole nature of the transition.[13] For the orientations obtained in ^{3}He induced reactions (at the incident energies of interest in the present work), all measured A_{44} values are expected to be zero within error. In general the knowledge of A_{22} alone does not result in unique spin assignments. Nevertheless A_{22} values used in conjunction with other observables can be useful, as will be discussed later.

C. $\gamma-\gamma$ coincidence measurement

The coincidence measurement was performed using two detectors positioned at 0° and 100° with respect to the beam axis. Gamma coincidences, subject to the proton coincidence requirement, were recorded event by event on magnetic tape. The data were then processed off-line, subtracting accidental coincidences. In processing the data we were concerned with obtaining reliable and quantitative coincidence intensities, particularly for weak coincidences. Uncertainties reflect not only statistics but various corrections which may be large. In the present work we have adopted new procedures to improve the accuracy of the coincidence analysis.

When gates are set on γ ray peaks prior to a tape search, one unavoidably encounters overlapping peaks. Peak areas extracted from the resultant coincidence spectra must then be corrected for the fact that these were contributions from more than one peak in the gate. The accuracy to which these overlap corrections can be made is sometimes poor because resolution has been lost by summing over one dimension of the original array. One can recover the resolution in this dimension by performing a second tape search where gates are set on the other γ-ray dimension of the array.

Corrections to coincidence intensities which arise from Compton scattering must also be made. The standard solution to this problem is to set gates on Compton background before the tape search. However, in complicated spectra there are few places that one can confidently set background windows so that interpolations between them have large uncertainties. In addition, a bad peak area in either of the background spectra produces errors in all spectra in between. We have devised a new scheme which makes use of the fact that a typical transition is not really in coincidence with most other transitions in the nucleus. Thus its peak area in most of the coincidence spectra, not just the background spectra, reflects the magnitude of the Compton contribution. Since a Compton distribution has a smooth energy dependence, spurious peaks due to it can readily be distinguished from real coincidence peaks, and the use of all available data results in much more reliable corrections.

III. THE LEVEL SCHEME

The level scheme deduced in the present work for ^{111}Ag is shown in Figs. 2 and 3. In the coincidence experiment 156 γ-rays were identified as belonging to ^{111}Ag and placed unambiguously in the level scheme. The level scheme contains 81 states, 37 of which are new. The low background in the proton-gated coincidence data allowed the placement of many weak transitions. The spin and parity assignments shown came from a combination of three sources: adopted values from Nuclear Data Sheets,[14] our excitation function analysis, and our angular distribution measurements.

The excitation function analysis gave very consistent re-

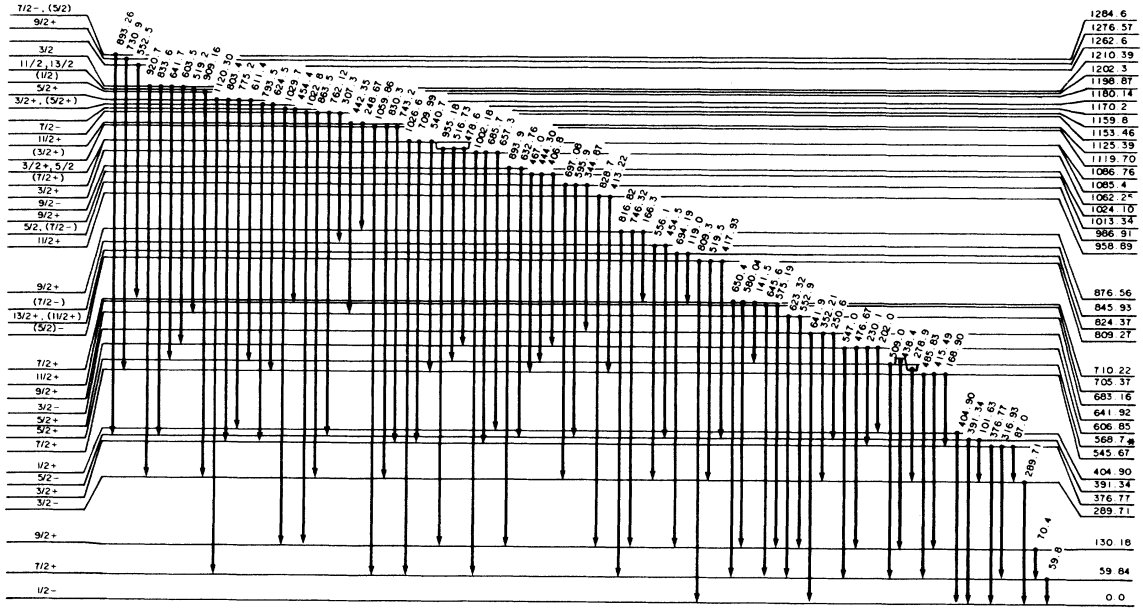

FIG. 2. The low energy portion of the level scheme deduced for ^{111}Ag. The asterisk by the 568.7-keV entry indicates that two states are present and are discussed in the text.

TABLE I. Reference slopes for excitation functions.

I_i	E_γ	Slope(Error)	Adopted slope range
$\frac{1}{2}$	404.9	−0.123(0.002)	−0.140(0.030)
	289.8	−0.055(0.002)	
$\frac{3}{2}$	376.7	−0.074(0.002)	−0.072(0.011)
	316.8	−0.099(0.017)	
	352.2	−0.077(0.008)	
$\frac{5}{2}$	476.7	−0.038(0.010)	−0.032(0.014)
	762.2	+ 0.000(0.006)	
	168.9	+ 0.005(0.008)	
$\frac{7}{2}$	415.5	+ 0.013(0.003)	+ 0.006(0.010)
	556.2	+ 0.002(0.016)	
	417.7	−0.010(0.007)	
$\frac{9}{2}$	632.8	+ 0.088(0.004)	+ 0.080(0.020)
	413.2	+ 0.173(0.008)	
$\frac{11}{2}$	1142.4	+ 0.185(0.036)	+ 0.150(0.030)
	575.2	+ 0.127(0.006)	

sults. Table I lists slopes (and errors) for transitions depopulating states of known spins. The slopes for these reference transitions fall clearly into groups which are well separated. When the slopes for all transitions were compared to the ones shown in Table I, the same distinct groupings were observed. This leads to the adopted slope ranges for different spins given in the last column of the table. We believe that the slopes result in reliable spin assignments when a particular value lies unambiguously in one of the ranges.

Although the A_{44} values were not measurable due to the small nuclear orientation in these experiments, the angular distribution measurements still gave useful spin and parity information in some cases. If the measured A_{22}

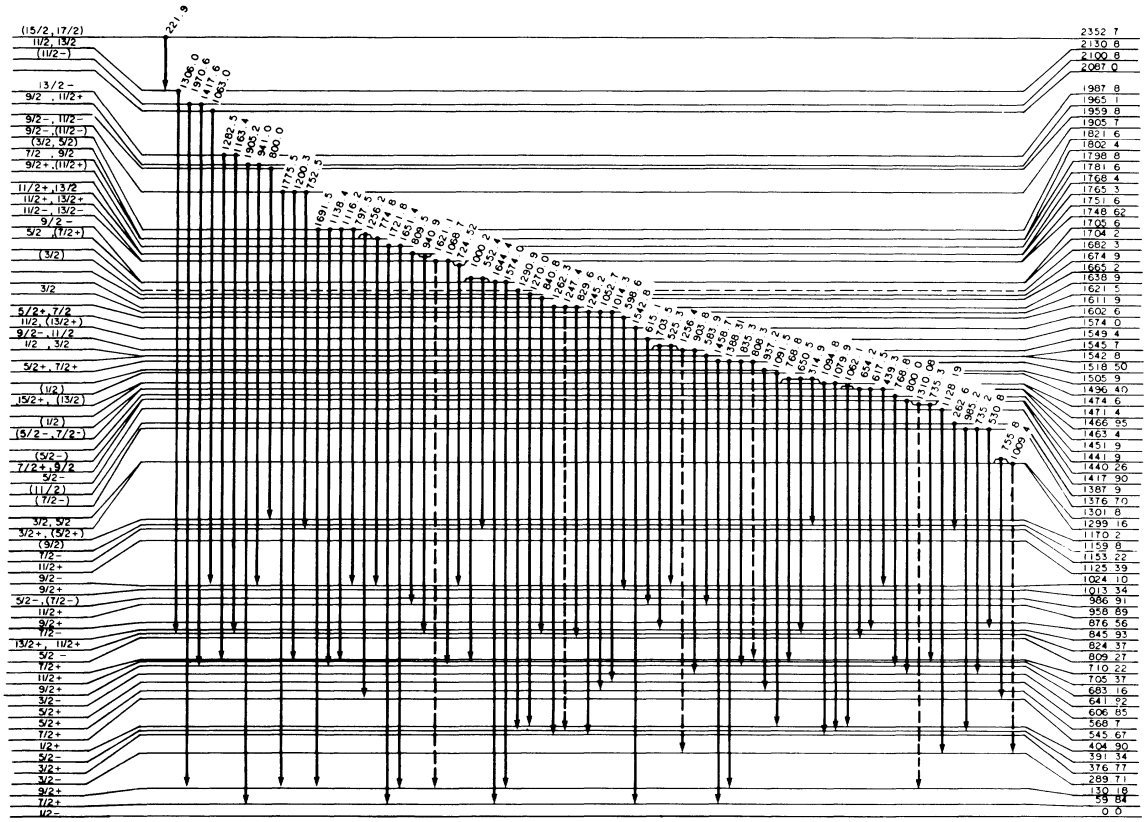

FIG. 3. The higher energy portion of the level scheme deduced for ^{111}Ag.

TABLE II. Extreme and unmixed A_{22}^0 values for different spin changes.

I_i	$\Delta I = 0$			$\Delta I = -1$			$\Delta I = +1$		
	$\delta+$	$\delta = 0$	$\delta-$	$\delta+$	$\delta = 0$	$\delta-$	$\delta+$	$\delta = 0$	$\delta-$
$\frac{3}{2}$	1.00	0.40	−0.60	1.00	−0.50	−1.00	−0.83	−0.10	0.38
$\frac{5}{2}$	0.76	0.46	−0.51	0.96	−0.40	−1.16	−0.99	−0.14	0.50
$\frac{7}{2}$	0.66	0.48	−0.45	0.92	−0.36	−1.19	−1.06	−0.17	0.57
$\frac{9}{2}$	0.61	0.49	−0.42	0.89	−0.33	−1.20	−1.09	−0.18	0.61
$\frac{11}{2}$	0.58	0.49	−0.41	0.87	−0.32	−1.20	−1.11	−0.19	0.63
$\frac{13}{2}$	0.56	0.49	−0.39	0.85	−0.31	−1.21	−1.12	−0.20	0.65

value is sufficiently large in magnitude, it can uniquely identify a $\Delta I = \pm 1$ transition. By comparing measured A_{22} values for known $E2$ transitions to the theoretical A_{22}^0 values, one finds that attenuations are typically 0.3 to 0.5. Thus, for example, a measured A_{22} more negative than −0.4 corresponds to an A_{22}^0 of at least −0.8. Table II gives extreme A_{22}^0 values for mixed $\Delta I = 0$ and $\Delta I = \pm 1$ transitions.

$A_{22} < -0.4$ uniquely identifies a $\Delta I = \pm 1$ transition. Similarly a large positive A_{22} specifies a $\Delta I = -1$ transition, except for small initial spins where $\Delta I = 0$ is possible. (A_{22}^0 values for $\Delta I = \pm 2$ transitions are not included in the table, since they are always less than 0.57.) A substantial mixing ratio also means that the transition does not change parity. The theoretical A_{22}^0 values for unmixed transitions are also included in Table II, and it is clear that a large measured A_{22} value rules out an $E1$ transition in all cases. Small measured A_{22} values can also demand a mixed $E2$-$M1$ transition if the spin change is known from some other measurement. An A_{22} of the opposite sign expected for an unmixed transition clearly indicates mixing. However, a small A_{22} of the same sign indicates mixing if the orientation of the initial state is known and the A_{22} is smaller than expected for a pure $E1$ transition.

The level scheme with pertinent supporting information is also presented in Table III. The first and third columns give the state and transition energies. The energies given with two fractional digits are believed known to better than 0.1 keV, while those given with one fractional digit are believed known within 0.5 keV. In the second and fourth columns we give the initial and final spin if determined. The fifth column gives the energy of the final state. The placement of transitions in the level scheme was based not only on the existence of coincidences but consistency of intensities feeding and depopulating a proposed state. The presence of unresolved γ rays was determined by comparing coincidence and singles intensities. Column six of the table gives the measured intensities of transitions in ^{111}Ag, and column seven gives contaminant intensities and their sources where known. The adopted intensities are the relative A_{00} values from the angular distribution measurement for uncontaminated transitions or coincidence intensities for contaminated transitions. In column eight the A_{22} values from the angular distribution measurements are given, and in column nine the excitation function slopes are listed. Column ten contains labels which indicate the source of the spin and parity assignment. If Nuclear Data Sheets had given a spin assignment, the label "N" is used. An "N" alone indicates that we have nothing to add from our data. In many cases we have been able to remove ambiguities from previous assignments or assign spins to new states. The label "E" means that we have used this excitation function slope to support the spin assignment, and the labels "A" and "A_π" indicate the use of our angular distribution to determine the spin and parity respectively. Most of the assignments given are explained by these labels alone in a straightforward fashion. However, a few spin assignments require specific discussion.

Our coincidence data show that the "state" previously deduced at 568.8 keV is actually two states. The arguments for the existence of this "state" were the placements of depopulating transitions of 278.8, 438.7, and 508.9 keV. Our data (and previous data[4]) show that transitions feeding the 568.8 keV-state are not in coincidence with the 278.8-keV transition. The 278.8-keV γ ray is in coincidence with the γ ray from the 289.7-keV state, so it definitely comes from a state at approximately 568 keV. In the present work we populate a new state at 1013.34 keV, which decays via a 444.30-keV transition. This transition shows no coincidence with the 438.8-keV transition, but is in coincidence with the 278.8-keV transition. Since the 438.7-keV transition is more intense than the 278.8-keV transition the coincidence data require two states at 568.5 keV and 568.8 keV. The 568.5-keV state must have positive parity since the 444.30-keV transition is nonparity changing, from its angular distribution, and depopulates the $\frac{9}{2}^+$ 1013.34-keV state. Since the 278.8-keV transition feeds a $\frac{3}{2}^-$ state we have assigned spin and parity $\frac{5}{2}^+$ to the 568.5-keV state. The feeding of the 568.8-keV state from the spin $\frac{3}{2}$ 1210.39-keV state and its decay to the 130.18-keV $\frac{9}{2}^+$ state limit its spin to $\frac{5}{2}$ or $\frac{7}{2}$. The feeding of the 568.8-keV state from the positive parity 1085.42-keV state by the mixed 516.73-keV transition requires positive parity for the 568.8-keV state. The angular distribution of the 516.73-keV transition slightly favors a $\frac{5}{2}^+$ assignment but is not conclusive. Therefore we assign spin and parity $(\frac{5}{2}, \frac{7}{2})^+$ to the 568.8-keV state.

The 1119.70-keV state has been assigned a spin of $\frac{3}{2}$ on the basis of the excitation function slope for the 1059.86-keV transition. Nuclear Data Sheets[14] had tentatively placed an 1120.3-keV transition depopulating both the

TABLE III. Analysis of γ rays emitted following the ^{110}Pd(^{3}He,pn)^{111}Ag reaction at 18 MeV.

E_i (keV)	I_i^π	E_γ	I_f^π	E_f	Intensities ^{111}Ag	Contaminants	A_{22}x100	Exc. func slope x 10^3	Data used
59.84[b]	$\frac{7}{2}^+$	59.8[a]	$\frac{1}{2}^-$	0.0					N
130.18[b]	$\frac{9}{2}^+$	70.4[a]	$\frac{7}{2}^+$	59.84					N
289.71	$\frac{3}{2}^-$	289.71	$\frac{1}{2}^-$	0.0	825(8)		−12(2)	−55(17)	N
376.77	$\frac{3}{2}^+$	376.77	$\frac{1}{2}^-$	0.0	664(7)		−8(2)	−74(2)	N
		316.93	$\frac{7}{2}^+$	59.84	22(1)		8(1)	−99(18)	
		87.0[a]	$\frac{3}{2}^-$	289.71	20(2)				
391.34	$\frac{5}{2}^-$	391.34	$\frac{1}{2}^-$	0.0	1000(9)		7(2)	−11(1)	N
		101.63	$\frac{3}{2}^-$	289.71	30(6)		34(31)	−47(15)	
404.90	$\frac{1}{2}^+$	404.90	$\frac{1}{2}^-$	0.0	323(6)		0(4)	−123(2)	N
545.67	$\frac{7}{2}^+$	485.83	$\frac{7}{2}^+$	59.84	112(2)		10(3)	31(6)	N
		415.49	$\frac{9}{2}^+$	130.18	369(5)		−6(3)	13(3)	
		168.90	$\frac{3}{2}^+$	376.77	125(5)		10(3)	6(8)	
568.5*	$\frac{5}{2}^+$	508.6	$\frac{7}{2}^+$	59.84	300(100)				
		278.8	$\frac{3}{2}^-$	289.71	15(4)				
568.8	$\frac{5}{2}^+,(\frac{7}{2}^+)$	509.0	$\frac{7}{2}^+$	59.84	400(100)				
		438.4	$\frac{9}{2}^+$	130.18	100(10)	12(5) ^{111}Ag	3(4)	−6(1)	
606.85	$\frac{5}{2}^+$	547.0	$\frac{7}{2}^+$	59.84	305(5)	95(5) ^{197}Au			
		476.67	$\frac{9}{2}^+$	130.18	62(1)		1(9)	−38(10)	
		230.1	$\frac{3}{2}^+$	376.77	19(3)	20(3)			
		202.0	$\frac{1}{2}^+$	404.90	14(3)		−17(25)		
641.92	$\frac{3}{2}^-$	641.92	$\frac{1}{2}^-$	0.0	230(5)	31(5) ^{111}Ag	−9(2)	−61(3)	N
		352.21	$\frac{3}{2}^-$	289.71	82(6)		8(6)	−77(8)	
		250.6	$\frac{5}{2}^-$	391.34	11(2)		49(18)	−95(38)	
683.16	$\frac{9}{2}^+$	623.32	$\frac{7}{2}^+$	59.84	346(4)	8(4) ^{111}Ag	2(3)	91(4)	N,E
		552.9	$\frac{9}{2}^+$	130.18	39(4)	12(4) ^{111}Ag			
705.37	$\frac{11}{2}^+$	645.5	$\frac{7}{2}^+$	59.84	22(3)		13(27)		N
		575.19	$\frac{9}{2}^+$	130.18	369(5)		11(2)	127(6)	E
710.22	$\frac{7}{2}^+$	650.4	$\frac{7}{2}^+$	59.84	80(4)	38(4) ^{111}Ag			N
		580.04	$\frac{9}{2}^+$	130.18	142(4)		−14(5)	−22(8)	A
		141.5	$\frac{5}{2}^+$	568.8	6(1)				
809.27	$\frac{5}{2}^-$	809.3	$\frac{1}{2}^-$	0.0	17(8)	15(3)			
		519.5	$\frac{3}{2}^-$	289.71	91(7)	42(4) ^{111}Ag			
		417.93	$\frac{5}{2}^-$	391.34	128(5)		3(5)	−11(7)	E,A_π
824.37	$\frac{13}{2}^+,\frac{11}{2}^+$	694.19	$\frac{9}{2}^+$	130.18	303(5)		20(3)	184(5)	E ,A_π
		119.0	$\frac{11}{2}^+$	705.37	15(5)				
845.93	$\frac{7}{2}^-$	556.22	$\frac{3}{2}^-$	289.71	42(2)		15(09)	2(16)	N,E
		454.6	$\frac{5}{2}^-$	391.34	203(6)	100(4) ^{111}Ag			
876.56	$\frac{9}{2}^+$	816.82	$\frac{7}{2}^+$	59.84	50(2)		56(8)	77(23)	A,E
		746.32	$\frac{9}{2}^+$	130.18	74(1)		1(4)	81(11)	E
		166.3	$\frac{7}{2}^+$	710.22	30(2)	18(3) ^{110}Ag			
958.89	$\frac{11}{2}^+$	828.7	$\frac{9}{2}^+$	130.18	6(2)				
		413.22	$\frac{7}{2}^+$	545.67	190(3)		26(4)	173(8)	E
986.91	$\frac{5}{2}^-,(\frac{7}{2}^-)$	697.08	$\frac{3}{2}^-$	289.71	48(3)		37(11)	−26(20)	E,A_π
		595.9	$\frac{5}{2}^-$	391.34	58(2)		14(6)	0(18)	E
		344.87	$\frac{3}{2}^-$	641.92	15(3)				
1013.34*	$\frac{9}{2}^+$	467.0	$\frac{7}{2}^+$	545.67	15(4)	28(4) ^{110}Cd			
		444.30	$\frac{5}{2}^+$	568.5	58(2)		30(6)	64(24)	E,A
		406.8	$\frac{5}{2}^+$	606.85	34(4)		43(23)	61(18)	E,A
1024.10	$\frac{9}{2}^-$	893.9	$\frac{9}{2}^+$	130.18	5(4)	35(8) ^{111}Ag			N
		632.76	$\frac{5}{2}^-$	391.34	260(4)		14(3)	89(44)	E
1062.2	$\frac{3}{2}^+$	1002.2	$\frac{7}{2}^+$	59.84	44(3)		4(12)	−110(16)	N,E
		685.7	$\frac{3}{2}^+$	376.77	39(1)		21(7)	−63(13)	E

TABLE III. (*Continued*).

E_i (keV)	I_i^π	E_γ	I_f^π	E_f	Intensities ^{111}Ag	Intensities Contaminants	A_{22}x100	Exc. func slope x 10^3	Data used
		657.3	$\frac{1}{2}^+$	404.90	17(5)	954 ^{110}Cd			
1085.4	$(\frac{7}{2}^+)$	955.18	$\frac{9}{2}^+$	130.18	51(2)		20(8)	39(17)	E,A$_\pi$
		516.73	$\frac{5}{2}^+$	568.8	33(1)		−3(7)	16(52)	
		478.63	$\frac{5}{2}^+$	606.85	18(4)		14(9)	5(30)	E,A$_\pi$
1086.76	$\frac{3}{2}^+,(\frac{5}{2})$	1026.6	$\frac{7}{2}^+$	59.84	7(1)		1(34)	−58(78)	N
		709.99	$\frac{3}{2}^+$	376.77	87(2)		−19(4)	−70(6)	E,A$_\pi$
		540.7	$\frac{7}{2}^+$	545.67	10(4)	16(4)			
1119.70	$(\frac{3}{2}^+)$	1059.86	$\frac{7}{2}^+$	59.84	37(2)		4(9)	−112(17)	E
		830.3	$\frac{3}{2}^-$	289.71	11(4)	12(3) ^{111}Ag			
		743.2	$\frac{3}{2}^+$	376.77	16(6)	14(6)			
1125.39*	$\frac{11}{2}^+$	442.35	$\frac{9}{2}^+$	683.16	63(2)		3(6)	171(28)	E,A$_\pi$
		248.67	$\frac{9}{2}^+$	876.56	19(4)		52(12)	289(75)	A
1153.46	$\frac{7}{2}^-$	1022.8	$\frac{9}{2}^+$	130.18	11(1)		3(17)	−32(63)	N
		863.5	$\frac{3}{2}^-$	289.71	6(3)	7(3)			
		762.12	$\frac{5}{2}^-$	391.34	101(2)		−20(3)	0(7)	E
		307.3	$\frac{7}{2}^-$	845.93	15(2)	10(2)			
1159.8		1029.7	$\frac{9}{2}^+$	130.18	18(2)				
		454.4	$\frac{11}{2}^+$	705.37	100(4)	203(6) ^{111}Ag			
1170.2	$\frac{3}{2}^+,(\frac{5}{2}^+)$	793.5	$\frac{3}{2}^+$	376.77	43(5)	14(3) ^{110}Cd	13(5)	−88(30)[c]	E
		624.5	$\frac{7}{2}^+$	545.67	8(4)	346(4) ^{111}Ag			
1180.14	$\frac{5}{2}^+$	1120.30	$\frac{7}{2}^+$	59.84	60(2)		8(5)	−32(12)	N,E
		803.4	$\frac{3}{2}^+$	376.77	7(3)	5(3)			
		775.2	$\frac{1}{2}^+$	404.90	11(4)	16(3) ^{111}Ag			
		611.4	$\frac{5}{2}^+$	568.8	10(1)		26(18)	−10(76)	
1198.87*	$(\frac{1}{2})$	909.16	$\frac{3}{2}^-$	289.71	55(1)		3(4)	−123(21)	E
1202.3*	$\frac{11}{2},\frac{13}{2}$	519.2	$\frac{9}{2}^+$	683.16	42(4)	91(7) ^{111}Ag		219(33)[c]	E
1210.39	$\frac{3}{2}$	920.70	$\frac{3}{2}^-$	289.71	24(1)		−13(10)	−100(2)	N,E
		833.6	$\frac{5}{2}^-$	391.34	8(6)	15(6)			
		641.7	$\frac{5}{2}^+$	568.8	31(5)	230(4) ^{111}Ag			
		603.5	$\frac{5}{2}^+$	606.85	9(2)	6(2)			
1262.6*		552.5	$\frac{7}{2}^+$	710.22	8(3)	41(2) ^{111}Ag			
1276.6*	$\frac{9}{2}^+$	730.9	$\frac{7}{2}^+$	545.67	47(4)	15(4)	−40(4)	65(14)	E,A
1284.6*	$\frac{7}{2}^-,(\frac{5}{2})$	893.3	$\frac{5}{2}^-$	391.34	35(8)	5(4) ^{111}Ag	24(7)	−6(16)	E,A$_\pi$
1299.16*	$\frac{5}{2}^-,\frac{7}{2}^-$	1009.45	$\frac{3}{2}^-$	289.71	47(5)		11(10)	−26(24)	E,A$_\pi$
1301.8*		755.8	$\frac{7}{2}^+$	845.93	10(3)	9(3) ^{111}Ag			
1376.7*	$\frac{7}{2}^-$	985.2	$\frac{5}{2}^-$	391.34	15(2)		26(26)	44(55)	E
		735.2	$\frac{3}{2}^-$	641.92	4(2)	7(2) ^{111}Ag			
		530.8	$\frac{7}{2}^-$	845.93	10(1)		39(28)	26(47)	E
1387.9*	$(\frac{11}{2})$	262.6	$\frac{11}{2}^+$	1153.22	16(4)	7(3) ^{110}Ag	36(6)	159(43)[c]	E
1417.90*	$\frac{5}{2}^-$	1128.19	$\frac{3}{2}^-$	289.71	45(4)		47(11)	−11(16)	E,A
1440.26*	$\frac{7}{2}^+,\frac{9}{2}$	1310.08	$\frac{9}{2}^+$	130.18	19(2)		26(15)	27(45)	E,A$_\pi$
		735.3	$\frac{11}{2}^+$	705.37	7(2)	4(2) ^{111}Ag			
1441.9*	$(\frac{5}{2}^-)$	800.0	$\frac{3}{2}^-$	641.92	11(2)	5(2) ^{111}Ag	75(23)	39(56)	A
1451.9*		768.8	$\frac{9}{2}^+$	638.16	25(4)	13(4)^{111}Ag			
1463.4	$(\frac{5}{2}^-,\frac{7}{2}^-)$	654.2	$\frac{5}{2}^-$	809.27	15(3)	8(3)	49(15)	−42(28)	A
		617.5	$\frac{7}{2}^-$	845.93	6(2)	9(2) ^{109}Ag,40(10)			
		439.3	$\frac{9}{2}^-$	1024.10	12(5)	100(10) ^{111}Ag			
1466.9*	$(\frac{1}{2})$	1062.1	$\frac{1}{2}^+$	404.90	28(5)		22(14)	−189(21)	E
1471.4*		1094.8	$\frac{3}{2}^+$	376.77	5(2)	7(2)	−31(23)	−2(46)	
		1079.9	$\frac{5}{2}^-$	391.34	6(5)	18(5)		−71(24)	

TABLE III. (*Continued*).

E_i (keV)	I_i^π	E_γ	I_f^π	E_f	Intensities ^{111}Ag	Intensities Contaminants	A_{22}x100	Exc. func slope x 10^3	Data used
1474.6*	$\frac{15}{2}^+,(\frac{13}{2}^+)$	768.8	$\frac{11}{2}^+$	705.37	13(4)	25(4) ^{111}Ag			
		650.5	$\frac{13}{2}^+,\frac{11}{2}^+$	824.37	38(4)	81(4) ^{111}Ag		400(100)[c]	E
		314.9		1159.8	5(1)		64(44)	194(4)	
1496.4*	$(\frac{1}{2})$	1091.5	$\frac{1}{2}^+$	404.90	10(3)	3(2) ^{110}Cd	53(37)	−160(30)[c]	E
1505.9		937.2	$\frac{5}{2}^+$	568.8	12(5)	210(5) ^{110}Cd			
1518.50	$\frac{5}{2}^+,\frac{7}{2}^+$	1458.7	$\frac{7}{2}^+$	59.84	17(1)		−15(15)	−30(54)	
		1388.32	$\frac{9}{2}^+$	130.18	36(1)		2(6)	−50(27)	N
		835.3	$\frac{9}{2}^+$	683.16	9(6)	13(6)			
1542.8		583.9	$\frac{11}{2}^+$	958.89	17(2)		103(25)	139(84)	
1545.7*	$\frac{1}{2},\frac{3}{2}$	1256.0	$\frac{3}{2}^-$	289.71	5(3)	9(3) ^{111}Ag			
		903.8	$\frac{3}{2}^-$	641.92	12(1)		3(18)	−109(54)	E
1549.4	$\frac{9}{2}^-,\frac{11}{2}^-$	703.5	$\frac{7}{2}^-$	958.89	13(2)	9(2)	30(13)	−31(27)	N
		525.3	$\frac{9}{2}^-$	1024.10	29(4)	13(4)	−32(8)	67(44)	A_π
1574.0*	$\frac{11}{2},(\frac{13}{2}^+)$	615.1	$\frac{11}{2}^+$	958.89	35(3)	7(3)	39(14)	148(26)	E,A_π
1602.6	$\frac{5}{2}^+,\frac{7}{2}$	1542.8	$\frac{7}{2}^+$	59.84	32(2)		6(12)	15(23)	E,A_π
1611.9*		598.6	$\frac{9}{2}^+$	1013.34	21(6)	4(2) ^{110}Cd, 17(6)			
1621.5	$\frac{3}{2}$	1245.2	$\frac{3}{2}^+$	376.77	7(3)	15(3)			N
		1052.7	$\frac{5}{2}^+$	568.8	14(4)	8(4)	3(9)	−138(26)	E
		1014.3	$\frac{5}{2}^+$	606.85	26(4)	16(4)	1(7)	−81(15)	E
1638.9*		1262.3	$\frac{3}{2}^+$	376.77	8(4)	7(4)	46(15)	−52(49)	
		1247.4	$\frac{5}{2}^-$	391.34	6(4)	7(4)	26(20)	−101(65)	
		829.6	$\frac{5}{2}^-$	809.27	3(2)	21(4) ^{111}Ag			
1665.2*		840.8	$\frac{13}{2}^+,\frac{11}{2}^+$	824.37	23(4)	3(2) ^{110}Cd, 21(4)	26(10)	103(28)	
1674.9	$(\frac{3}{2})$	1270.0	$\frac{1}{2}^+$	404.90	7(4)		−20(27)	−6(40)	A
1682.3*		1290.9	$\frac{5}{2}^-$	391.34	13(5)	8(5)	−2(12)	−38(33)	
1704.2	$\frac{5}{2},(\frac{7}{2}^+)$	1644.4	$\frac{7}{2}^+$	59.84	13(1)		−38(20)	43(58)	A
		1574.0	$\frac{9}{2}^+$	130.18	19(2)		13(14)	−14(34)	E
1705.6	$\frac{9}{2}^-$	1000.2	$\frac{11}{2}^+$	705.37	3(2)	3(2)			
		718.7[a]	$\frac{5}{2}^-$	986.91					
		552.4	$\frac{7}{2}^-$	1153.22	4(3)	8(4) ^{111}Ag, 39(4)			
1748.62*	$\frac{11}{2}^-,\frac{13}{2}^-$	724.52	$\frac{9}{2}^-$	1024.10	36(1)		19(6)	177(28)	E,A_π
1751.6*	$\frac{11}{2}^+,\frac{13}{2}^+$	1621.1	$\frac{9}{2}^+$	130.18	17(2)		29(16)	177(50)	E,A_π
		1068.7	$\frac{9}{2}^+$	683.16	11(4)	6(4)	52(25)	144(56)	A
1765.3*	$\frac{11}{2}^+,\frac{13}{2}$	940.9	$\frac{13}{2}^+,\frac{11}{2}^+$	824.37	22(5)	3(2) ^{111}Ag	28(11)	172(59)[c]	E,A_π
1768.4*		809.5	$\frac{11}{2}^+$	958.89	11(4)	23(4)			
1781.7	$\frac{9}{2}^+,(\frac{11}{2}^+)$	1721.8	$\frac{7}{2}^+$	59.84	17(2)		10(19)	119(53)	N,A_π
		1651.4	$\frac{9}{2}^+$	130.18	21(2)		25(17)	47(53)	A
1798.8*	$\frac{7}{2},\frac{9}{2}$	774.8	$\frac{9}{2}^-$	1024.10	16(3)	11(4) ^{111}Ag	21(10)	40(35)[c]	E
1802.4*	$(\frac{3}{2},\frac{5}{2})$	1256.7	$\frac{7}{2}^+$	545.67	9(3)	5(3) ^{111}Ag, 6(3)	−1(11)	−86(54)[c]	E
1821.6	$\frac{9}{2}^-,(\frac{11}{2}^-)$	1691.5	$\frac{9}{2}^+$	130.18	15(2)		4(22)	74(43)	N,E
		1138.4	$\frac{9}{2}^+$	683.16	9(2)		66(50)	151(68)	E
		1116.2	$\frac{11}{2}^+$	705.37	5(2)	21(3) ^{110}Cd, 19(3)			
		797.5	$\frac{9}{2}^-$	1024.10	5(2)	9(2)			
1905.7	$\frac{9}{2}^-,\frac{11}{2}^-$	1775.5	$\frac{9}{2}^+$	130.18	8(2)	4(2)		274(38)	N
		1200.3	$\frac{11}{2}^+$	705.37	4(2)	12(2)			
		752.5	$\frac{7}{2}^-$	1153.22	3(1)	9(1)			
1959.8*		800.0	$(\frac{9}{2}^+)$	1159.8	5(2)	11(2) ^{111}Ag			
1965.1	$\frac{9}{2},\frac{11}{2}^+$	1905.2	$\frac{7}{2}^+$	59.84	8(2)				
		941.0	$\frac{9}{2}^-$	1024.10	3(2)	17(3) ^{111}Ag			
1987.8	$\frac{13}{2}^-$	1282.5	$\frac{11}{2}^+$	705.37	13(3)	4(3)	1(14)	246(68)	N,E

TABLE III. (*Continued*).

E_i (keV)	I_i^π	E_γ	I_f^π	E_f	Intensities ^{111}Ag	Contaminants	A_{22}x100	Exc. func slope x 10^3	Data used
		1163.4	$\frac{13}{2}^+, \frac{11}{2}^+$	824.37	4(2)	13(4) ^{110}Cd			
2087.0		1063.0	$\frac{9}{2}^-$	1024.10	6(2)	28(5) ^{111}Ag			
2100.8	$(\frac{11}{2}^-)$	1970.6	$\frac{9}{2}^+$	130.18	30(8)				N
		1417.6	$\frac{9}{2}^+$	683.16	4(3)				
2130.8*	$\frac{11}{2}, \frac{13}{2}$	1306.4	$\frac{13}{2}^+, \frac{11}{2}^+$	824.37	26(2)		−13(12)	171(53)	E
2352.7*	$(\frac{15}{2}, \frac{17}{2})$	221.9	$\frac{11}{2}, \frac{13}{2}$	2130.8	6(2)	5(2)	10(17)	295(80)	E

*New observed states.

[a]Gamma rays not observed experimentally in our work, but known from other works (Ref. 2).

[b]The state energy has been deduced from feeding transitions.

[c]Excitation function slopes have been corrected for known contamination.

1119.70- and 1180.4-keV states. Our excitation functions show that the 1120.3- and 1059.86-keV γ rays cannot come from the same state. Therefore we have placed the 1120.3-keV transition depopulating the 1180.4-keV state only.

We have assigned a spin of $\frac{3}{2}$ to the 1621.5-keV state because of the large negative excitation function slopes of the 1052.7- and 1014.3-keV transition coming from the state. Although both transitions are contaminated, it is very unlikely that contamination would cause both slopes to be so negative.

The state at 1674.6-keV has been assigned spin $(\frac{3}{2})$ on the following basis. The logft (7.2) of the β-decay feed from a $\frac{5}{2}^+$ state[4] eliminates spin $\frac{1}{2}^+$. The 1270.0-keV decay to a $\frac{1}{2}^+$ state eliminates a $\frac{7}{2}$ assignment, and the negative A_{22} for the transition eliminated a $\frac{5}{2}$ spin. The spin assignment is left uncertain because the transition is very weak.

The state at 1705.6 keV has been assigned spin and parity $\frac{9}{2}^-$. The state decays to $\frac{5}{2}^-$ and $\frac{11}{2}^+$ states, which restricts its spin and parity to $\frac{9}{2}^-$ or $\frac{7}{2}^+$. The state is fed in β-decay from an $\frac{11}{2}^-$ state with a logft of 7.3,[14] which eliminates the $\frac{7}{2}^+$ possibility.

Finally the state at 1965.1 keV has been assigned spin $\frac{9}{2}$ or $\frac{11}{2}^+$ because of the decay to a $\frac{7}{2}^+$ state and the β-decay feed from an $\frac{11}{2}^-$ state with a logft value of 6.8.[14]

IV. DISCUSSION AND INTERPRETATION

There are several indications that ^{111}Ag is more deformed than lighter Ag isotopes. The energy of the first-excited 2^+ state of the ^{110}Pd core (374 keV) is lower than that of lighter even-even Pd nuclei (e.g., 556 keV in ^{104}Pd), suggesting a larger deformation of the core. The low lying $\frac{1}{2}^+$ and $\frac{3}{2}^+$ state in ^{111}Ag, at 404 keV and 376 keV respectively, have no counterpart in lighter Ag isotopes. The occurrences of these low-lying states would follow naturally if ^{111}Ag were deformed. The Nilsson diagram appropriate for odd protons in ^{111}Ag is shown in Fig. 4. At deformations of $\delta = 0.18$ or greater, the $Z = 50$ shell closure disappears, and Nilsson states with $g_{7/2}$ and $d_{5/2}$ parentage are expected at comparable excitation energies to those of $g_{9/2}$ parentage. There has been, in previous work,[4,5] speculation about a rotational band based on this $\frac{1}{2}^+$[431] orbital. Finally the low-lying negative parity states appear to group by energies into three rotational bands with bandhead spin $\frac{1}{2}^-$, $\frac{3}{2}^-$, and $\frac{5}{2}^-$ respectively. Again, Fig. 4 shows that the negative parity Nilsson states expected nearest the Fermi surface for 47 protons are the $\frac{1}{2}^-$[301], the $\frac{3}{2}^-$[301], and the $\frac{5}{2}^-$[303] states for a deformation of $\delta = 0.2$. For these reasons the use of a rotational model for the interpretation of the structure observed in ^{111}Ag seemed natural.

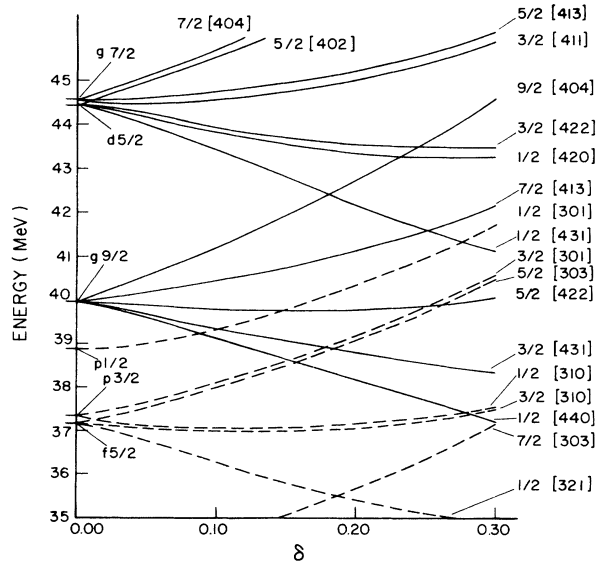

FIG. 4. Nilsson diagram for odd protons in ^{111}Ag.

The particular rotational model utilized was a symmetric rotor plus particle model. Suggestions have been made that the treatment of transitional nuclei, including odd-A Ag nuclei, requires an asymmetric rotor.[15] We believe that our results will show that this extra degree of freedom is not necessary. The calculation of energies and wave functions was the same as that used by Smith and Rickey[16] for Pd nuclei. The calculation of electromagnetic transition properties is the same used by Popli *et al.*[17] in interpreting ^{105}Ag and ^{107}Ag.

This specific model utilizes a rotational Hamiltonian in the strong-coupling limit modified to include a variable moment-of-inertia (VMI).[18] The basis states are thus rotational states built on Nilsson single-particle states,[9] characterized by good K and Ω, the projection of the total angular momentum **I** and the particle angular momentum **j** on the symmetry axis respectively. Pairing is treated by the BCS formalism. The Coriolis and recoil terms, which mix these states, are treated to all order. These terms were attenuated by a factor of 0.8. We would like to emphasize that this basic model has been used for years to interpret strongly deformed nuclei. Aside from differences in inertial quantities, the only deviation of its predictions from the familiar patterns seen in strongly deformed nuclei are due to the role of the Coriolis interaction.

The parameters κ and μ used for the Nilsson calculation were $\kappa = 0.06$ and $\mu = 0.48$ for the positive parity $N=4$ states and $\kappa=0.06$ and $\mu=0.532$ for the negative parity $N=3$ states. These parameters gave energies at zero deformation consistent with those tabulated by Reehal and Sorenson.[19]

A deformation of $\delta = 0.20$ was selected on the basis of measured $B(E2)$ values[4] and the Nilsson states near the Fermi surface. At this deformation the 47 protons in ^{111}Ag would place the Fermi surface between the $\frac{1}{2}^-[301]$ and $\frac{7}{2}^+[413]$ orbitals, with the $\frac{1}{2}^+[431]$ orbital lying slightly higher. The Fermi energy λ was finally taken to be 40.8 MeV and the pairing parameter Δ was set at $\Delta = 1.2$ MeV.

The basis states for the calculation were restricted to the Nilsson states near the Fermi surface. For negative parity these were the states with $p_{1/2}$, $p_{3/2}$, and $f_{5/2}$ parentage, the $\frac{1}{2}^-[301]$, $\frac{1}{2}^-[310]$, $\frac{1}{2}^-[321]$, $\frac{3}{2}^-[301]$, $\frac{3}{2}^-[312]$, and $\frac{5}{2}^-[303]$ states. For positive parities all states of $g_{9/2}$ parentage ($\frac{1}{2}^+[440]$, $\frac{3}{2}^+[431]$, $\frac{5}{2}^+[422]$, $\frac{7}{2}^+[413]$, and $\frac{9}{2}^+[404]$) were included, as well as the $\frac{1}{2}^+[431]$ and $\frac{3}{2}^+[422]$ states of $g_{7/2}$ and the $\frac{1}{2}^+[420]$ state of $d_{5/2}$ parentage. There were thus three "classes" of states in the basis, and as in the interpretation of strongly deformed nuclei, we found that the bands of each class required different moments of inertia. The VMI (Ref. 18) inertial parameters used were $\mathcal{I}_0 = 0$ and $C = 0.01$ for all negative parity $N = 3$ states. $\mathcal{I}_0 = 0$ and $C = 0.05$ for the $N = 4$ states of $g_{9/2}$ parentage, and $\mathcal{I}_0 = 10$ and $C = 0.01$ for $N = 4$ states of $g_{7/2}$ and $d_{5/2}$ parentage. These three sets of parameters may appear very different, but result in moments of inertia (for a given spin) which differ by only 50%.

In the comparison of the results of the calculation to the experimental results, emphasis has been placed on electromagnetic decay properties. Energies alone are not a sufficient basis for comparison, since frequently there are several states of the same spin and parity which have similar excitation energies. The comparison of experimental and calculated branching ratios provides a more reliable identification.

Table IV presents the comparison of experimental and calculated results for ^{111}Ag. This table includes only the experimental states which have been identified on the basis of their energies and branching ratios as corresponding to rotational states predicted by this model. Columns 1 and 2 give the experimental and theoretical initial energies for each state, and column 3 gives the initial spin. The model identification of the initial state is given in column 8. In the calculation we considered decay probabilities to all final states to which transitions were possible on the basis of energies and spin changes. However, the table only includes branches which were either observed or predicted to be observable. The fact that an unobserved but "allowed" branch was predicted to be statistically zero is a significant element of the identification, but if all of these possibilities were included the table would be uncomfortably large. For the branches included, column 4 gives the final spin and column 5 the γ-ray energy rounded to the nearest keV. Columns 6 and 7 give the experimental and theoretical branching ratios, and column 9 gives the model identification for each final state.

Three negative-parity rotational bands have been identified, with bandheads $\frac{1}{2}^-$, $\frac{3}{2}^-$, and $\frac{5}{2}^-$. These three bands are shown in Fig. 5. The experimental energy levels and γ-ray transitions are included in the figure, and the calculated energies are given by the black dots. The overall energy agreement is seen to be quite good. According to the calculation the three bands are relatively

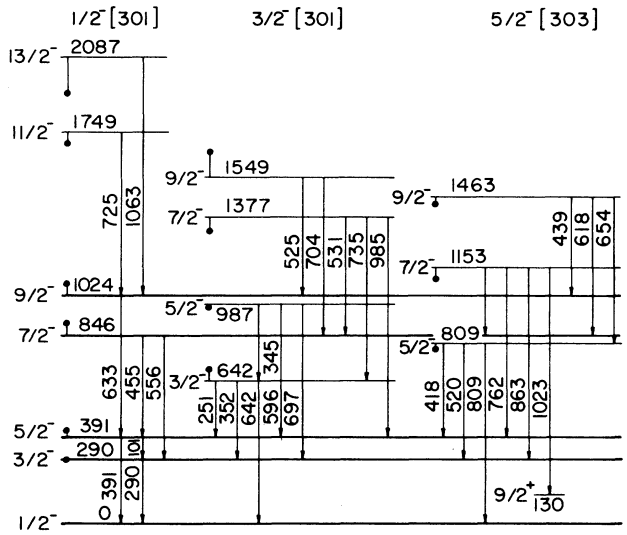

FIG. 5. States identified as members of negative parity rotational bands in ^{111}Ag. The dots represent energies calculated by the particle-rotor model.

TABLE IV. Comparison of experimental and calculated results for ^{111}Ag.

E_i (keV)		I_i^π	I_f^π	E_γ (keV)	Branching ratio		Theoretical identification	
Expt	Theor				Expt	Theor	Initial state	Final state
0.0	0[a]	$\frac{1}{2}^-$					$\frac{1}{2}^-[301]$	
59.84	74	$\frac{7}{2}^+$	$\frac{1}{2}^-$	60	1.0	1.0	$g_{9/2},R=2$	$\frac{1}{2}^-[301]$
130.18	130[a]	$\frac{9}{2}^+$	$\frac{7}{2}^+$	70	1.0	1.0	$g_{9/2},R=0$	$g_{9/2},R=2$
289.71	290	$\frac{3}{2}^-$	$\frac{1}{2}^-$	290	1.0	1.0	$\frac{1}{2}^-[301]$	$\frac{1}{2}^-[301]$
376.77	368	$\frac{3}{2}^+$	$\frac{1}{2}^-$	377	0.94	1.0	$\frac{1}{2}^+[431]$	$\frac{1}{2}^-[301]$
			$\frac{7}{2}^+$	317	0.03	0.0		$g_{9/2},R=2$
			$\frac{3}{2}^-$	87	0.03	0.0		$\frac{1}{2}^-[301]$
391.34	414	$\frac{5}{2}^-$	$\frac{1}{2}^-$	391	0.95	0.79	$\frac{1}{2}^-[301]$	$\frac{1}{2}^-[301]$
			$\frac{3}{2}^-$	101	0.05	0.21		$\frac{1}{2}^-[301]$
404.90	408	$\frac{1}{2}^+$	$\frac{1}{2}^-$	405	1.0	1.0	$\frac{1}{2}^+[431]$	$\frac{1}{2}^-[301]$
545.67	587	$\frac{7}{2}^+$	$\frac{7}{2}^+$	486	0.18	0.24	$\frac{1}{2}^+[431]$	$g_{9/2},R=2$
			$\frac{9}{2}^+$	415	0.61	0.75		$g_{9/2},R=0$
			$\frac{3}{2}^+$	169	0.21	0.01		$\frac{1}{2}^+[431]$
568.8	429	$\frac{5}{2}^+$	$\frac{7}{2}^+$	509	0.80	0.99	$g_{9/2},R=2$	$g_{9/2},R=2$
			$\frac{9}{2}^+$	438	0.20	0.01		$g_{9/2},R=0$
606.85	644	$\frac{5}{2}^+$	$\frac{7}{2}^+$	547	0.76	0.39	$\frac{1}{2}^+[431]$	$g_{9/2},R=2$
			$\frac{9}{2}^+$	477	0.15	0.00		$g_{9/2},R=0$
			$\frac{3}{2}^+$	230	0.06	0.60		$\frac{1}{2}^+[431]$
			$\frac{1}{2}^+$	202	0.03	0.01		$\frac{1}{2}^+[431]$
641.92	690	$\frac{3}{2}^-$	$\frac{1}{2}^-$	642	0.71	0.82	$\frac{3}{2}^-[301]$	$\frac{1}{2}^-[301]$
			$\frac{3}{2}^-$	352	0.25	0.16		$\frac{1}{2}^-[301]$
			$\frac{5}{2}^-$	251	0.04	0.02		$\frac{1}{2}^-[301]$
683.16	890	$\frac{9}{2}^+$	$\frac{7}{2}^+$	623	0.90	0.93	$g_{9/2},R=2$	$g_{9/2},R=2$
			$\frac{9}{2}^+$	553	0.10	0.07		$g_{9/2},R=0$
705.37	537	$\frac{11}{2}^+$	$\frac{7}{2}^+$	646	0.04	0.17	$g_{9/2},R=2$	$g_{9/2},R=2$
			$\frac{9}{2}^+$	575	0.96	0.83		$g_{9/2},R=0$
809.27	781	$\frac{5}{2}^-$	$\frac{1}{2}^-$	809	0.07	0.01	$\frac{5}{2}^-[303]$	$\frac{1}{2}^-[301]$
			$\frac{3}{2}^-$	520	0.39	0.59		$\frac{1}{2}^-[301]$
			$\frac{5}{2}^-$	418	0.54	0.40		$\frac{1}{2}^-[301]$
824.37	902	$\frac{13}{2}^+$	$\frac{9}{2}^+$	694	0.95	0.95	$g_{9/2},R=2$	$g_{9/2},R=0$
			$\frac{11}{2}^+$	119	0.05	0.05		$g_{9/2},R=2$
845.93	909	$\frac{7}{2}^-$	$\frac{3}{2}^-$	556	0.11	0.14	$\frac{1}{2}^-[301]$	$\frac{1}{2}^-[301]$
			$\frac{5}{2}^-$	455	0.89	0.86		$\frac{1}{2}^-[301]$
958.89	1011	$\frac{11}{2}^+$	$\frac{9}{2}^+$	829	0.10	0.24	$\frac{1}{2}^+[431]$	$g_{9/2},R=0$
			$\frac{7}{2}^+$	413	0.90	0.76		$\frac{1}{2}^+[431]$
986.91	976	$\frac{5}{2}^-$	$\frac{3}{2}^-$	697	0.40	0.50	$\frac{3}{2}^-[301]$	$\frac{1}{2}^-[301]$
			$\frac{5}{2}^-$	596	0.48	0.44		$\frac{1}{2}^-[301]$
			$\frac{3}{2}^-$	345	0.12	0.06		$\frac{3}{2}^-[301]$
1024.10	1089	$\frac{9}{2}^-$	$\frac{9}{2}^+$	894	0.02	0.0	$\frac{1}{2}^-[301]$	$g_{9/2},R=0$
			$\frac{5}{2}^-$	633	0.98	0.97		$\frac{1}{2}^-[301]$
1085.42	1113	$\frac{7}{2}^+$	$\frac{7}{2}^+$	1026	<0.1	0.24	$g_{9/2},R=4$	$g_{9/2},R=2$
			$\frac{9}{2}^+$	955	0.50	0.53		$g_{9/2},R=0$
			$\frac{5}{2}^+$	517	0.32	0.10		$g_{9/2},R=2$
			$\frac{5}{2}^+$	479	0.18	0.02		$\frac{1}{2}^+[431]$
			$\frac{9}{2}^+$	402	<0.03	0.11		$g_{9/2},R=2$
1153.46	1087	$\frac{7}{2}^-$	$\frac{9}{2}^+$	1023	0.08	0.03	$\frac{5}{2}^-[303]$	$g_{9/2},R=0$
			$\frac{3}{2}^-$	864	0.05	0.01		$\frac{1}{2}^-[301]$
			$\frac{5}{2}^-$	762	0.76	0.79		$\frac{1}{2}^-[301]$
			$\frac{7}{2}^-$	307	0.11	0.13		$\frac{1}{2}^-[301]$
1180.14	1223	$\frac{5}{2}^+$	$\frac{7}{2}^+$	1120	0.68	0.48	$g_{9/2},R=4$	$g_{9/2},R=2$
			$\frac{3}{2}^+$	803	0.08	0.31		$\frac{1}{2}^+[431]$

TABLE IV. (*Continued*).

E_i (keV) Expt	E_i (keV) Theor	I_i^π	I_f^π	E_γ (keV)	Branching ratio Expt	Branching ratio Theor	Theoretical identification Initial state	Theoretical identification Final state
			$\frac{1}{2}^+$	775	0.12	0.00		$\frac{1}{2}^+[431]$
			$\frac{5}{2}^+$	611	0.12	0.22		$g_{9/2}, R=2$
1276.6	1074	$\frac{9}{2}^+$	$\frac{7}{2}^+$	1217	<0.15	0.10	$\frac{1}{2}^+[431]$	$g_{9/2}, R=2$
			$\frac{7}{2}^+$	731	1.0	0.74		$\frac{1}{2}^+[431]$
			$\frac{5}{2}^+$	670	<0.05	0.13		$\frac{1}{2}^+[431]$
1376.7	1308	$\frac{7}{2}^-$	$\frac{5}{2}^-$	985	0.52	0.64	$\frac{3}{2}^-[301]$	$\frac{1}{2}^-[301]$
			$\frac{3}{2}^-$	735	0.14	0.02		$\frac{3}{2}^-[301]$
			$\frac{7}{2}^-$	531	0.34	0.24		$\frac{1}{2}^-[301]$
1463.4	1436	$\frac{9}{2}^-$	$\frac{5}{2}^-$	654	0.45	0.15	$\frac{5}{2}^-[303]$	$\frac{5}{2}^-[303]$
			$\frac{7}{2}^-$	618	0.18	0.49		$\frac{1}{2}^-[301]$
			$\frac{9}{2}^-$	439	0.36	0.35		$\frac{1}{2}^-[301]$
1474.6	1567	$\frac{15}{2}^+$	$\frac{11}{2}^+$	769	0.19	0.25	$g_{9/2}, R=4$	$g_{9/2}, R=2$
			$\frac{13}{2}^+$	651	0.81	0.71		$g_{9/2}, R=2$
1496.4	1489	$\frac{1}{2}^+$	$\frac{1}{2}^+$	1092	1.0	0.98	$\frac{1}{2}^+[420]$	$\frac{1}{2}^+[431]$
1542.8	1605	$\frac{15}{2}^+$	$\frac{11}{2}^+$	584	1.0	1.0	$\frac{1}{2}^+[431]$	$\frac{1}{2}^+[431]$
1549.4	1665	$\frac{9}{2}^-$	$\frac{7}{2}^-$	704	0.30	0.45	$\frac{3}{2}^-[301]$	$\frac{1}{2}^-[301]$
			$\frac{9}{2}^-$	525	0.70	0.43		$\frac{1}{2}^-[301]$
1574.0	1630	$\frac{13}{2}^+$	$\frac{11}{2}^+$	615	1.0	1.0	$\frac{1}{2}^+[431]$	$\frac{1}{2}^+[431]$
1748.62	1699	$\frac{11}{2}^-$	$\frac{7}{2}^-$	904	<0.06	0.31	$\frac{1}{2}^-[301]$	$\frac{1}{2}^-[301]$
			$\frac{9}{2}^-$	725	1.0	0.66		$\frac{1}{2}^-[301]$
1751.6	1724	$\frac{11}{2}^+$	$\frac{7}{2}^+$	1692	<0.25	0.10	$g_{9/2}, R=4$	$g_{9/2}, R=2$
			$\frac{9}{2}^+$	1621	0.61	0.61		$g_{9/2}, R=0$
			$\frac{9}{2}^+$	1069	0.39	0.11		$g_{9/2}, R=2$
			$\frac{13}{2}^+$	927	<0.11	0.12		$g_{9/2}, R=2$
1781.7[b]	1629	$\frac{9}{2}^+$	$\frac{7}{2}^+$	1722	0.29	0.63	$g_{9/2}, R=4$	$g_{9/2}, R=2$
			$\frac{9}{2}^+$	1651	0.61	0.24		$g_{9/2}, R=0$
			$\frac{9}{2}^+$	1099	0.12	0.05		$g_{9/2}, R=2$
2087.0	1919	$\frac{13}{2}^-$	$\frac{9}{2}^-$	1063	1.0	0.98	$\frac{1}{2}^-[301]$	$\frac{1}{2}^-[301]$

[a]The theoretical energies for the lowest $\frac{1}{2}^-$ and $\frac{9}{2}^+$ states have been adjusted to the experimental ones.

[b]Experimental branching ratios from Ref. 2 have been used because of the low γ-ray intensities in the present work.

pure Nilsson bands. The calculated wave function for members of the $\frac{1}{2}^-$ band are better than 98% $\frac{1}{2}^-[301]$, so that the result is an essentially pure $\Omega = \frac{1}{2}$ band with a decoupling parameter of $a = 0.54$. The Coriolis interaction has caused some mixing for the $\frac{3}{2}^-$ and $\frac{5}{2}^-$bands, although the wave function contains a dominant Nilsson component. Members of the $\frac{3}{2}^-$ band are better than 73% $\frac{3}{2}^-[301]$, while the $\frac{5}{2}^-$ band is shown to be better than 73% $\frac{5}{2}^-[303]$. Thus Table IV identifies the bands as $\frac{3}{2}^-[301]$ and $\frac{5}{2}^-[303]$ respectively. However, states in both the $\frac{3}{2}^-$ and $\frac{5}{2}^-$ bands decay in a manner which would seem uncharacteristic of rotational bands. The dominant decay modes for members of both bands are not intraband transitions, but are in fact $M1$ transitions to members of the $\frac{1}{2}^-$ band. In our model the physics responsible for the dominance of the interband $M1$ transitions is quite simple. For pure Nilsson bands, with no Coriolis mixing, transition probabilities for interband $M1$ transitions between the $\frac{3}{2}^-[301]$ and $\frac{1}{2}^-[301]$ bands would be very large since they are spin-flip transitions, typically 20–100 times larger than calculated probabilities of intraband $M1$ transitions in pure $\frac{3}{2}^-[301]$ and $\frac{5}{2}^-[303]$ bands. As a result of Coriolis mixing, the $\sim 25\%$ component of $\frac{3}{2}^-[301]$ in the $\frac{5}{2}^-$ band is enough to cause members of the $\frac{5}{2}^-$ band to decay predominantly to members of the $\frac{1}{2}^-$ band through the $\frac{3}{2}^-[301]$ component even though the band is still primarily a $\frac{5}{2}^-[303]$ Nilsson band.

In Table IV we have also identified a positive parity rotational band with a bandhead spin of $\frac{1}{2}^+$. The experi-

mental energy levels and γ-ray transitions associated with this band are shown in the right hand part of Fig. 6, with the calculated energies again given by black dots. The agreement between experimental and calculated observables is very good, except for the $\frac{9}{2}^+$ member, which for this reason is dashed in the figure. The energy mismatch is $\sim$200 keV, which is worse than that for other members of the band. The tentative association has been made because the 1277-keV state is the only known $\frac{9}{2}^+$ state in the energy region which has decay properties in reasonable agreement with those predicted. On the basis of energy there are better candidates, such as the 1013-keV $\frac{9}{2}^+$ state, but they have very different branching ratios. The calculation predicts this band to be a relatively pure $\frac{1}{2}^+$[431] Nilsson band with a decoupling parameter of $a = -1.141$, which is primarily responsible for the staggered spin sequence in the band (i.e., $\frac{3}{2}^+$, $\frac{1}{2}^+$, $\frac{7}{2}^+$, $\frac{5}{2}^+$, etc). As was mentioned earlier, the $\frac{1}{2}^+$[431] Nilsson state has $g_{7/2}$ parentage, and at small deformations would lie at very high excitation energies because of the $Z = 50$ shell closure. The existence of this band at low excitation energies is a strong signature of the deformation of ^{111}Ag.

For the state discussed above the model has predicted regular rotational bands characterized by a dominant Ω because Coriolis mixing has been small. Neither **R**, the rotational angular momentum of the core, or **j**, the angular momentum of the odd particle, has been a good quantum number. If, however, the Coriolis interaction has large effects, the low-lying final states of the calculation normally contain a dominant R and j rather than a dominant Ω. A group of states with the same R and j would have a spin **I** in the range $|R-j| \leq I \leq R+j$, and the number of states would be given by $2j+1 (R > j)$ or $2R+1 (R < j)$. The average excitation energy of one of these groups increases with R as expected from the core. Thus the predictions of the rotational model resemble particle-core multiplets rather than bands. Even at the deformation assumed here, Coriolis effects can be large for high values of j. At a deformation of $\delta = 0.20$, all five Nilsson states of $g_{9/2}$ parentage are essentially single-valued in j, and for the states nearest the Fermi surface the states have a $j=\frac{9}{2}$ component of better than 96%. The rotational calculation indeed predicts "multiplets" due to the Coriolis mixing of these basis states. As a quantitative example of this phenomena, the calculation predicts the $\frac{9}{2}^+$ member of the $j=\frac{9}{2}$, $R=2$ "multiplet" to be 97% $j=\frac{9}{2}$ and 85% $R=2$, but to have roughly comparable components of all five Ω values from $\frac{1}{2}$ to $\frac{9}{2}$.

Twelve states are identified as members of $j=\frac{9}{2}$ rotational multiplets in Table IV, and shown in the center part of Fig. 6. The lowest $\frac{9}{2}^+$ state has been identified as the $j=\frac{9}{2}$, $R=0$ state. The lowest $\frac{7}{2}^+$ state and the four states between 569 and 1180 keV have been identified as the complete $j=\frac{9}{2}$, $R=2$ "multiplet." Finally the top group of states in this center part of Fig. 6 have been identified as six of the nine members of the $j=\frac{9}{2}$, $R=4$ "multiplet." There are several known states of the right spin and energy to be candidates for the missing $\frac{3}{2}^+$ and $\frac{13}{2}^+$ members (three $\frac{3}{2}^+$ and three $\frac{13}{2}^+$ states), but they do not have the expected decay properties.

In a rotational calculation the relative energies of members of a multiplet depend on the nature of the Coriolis interaction and the position of the Fermi surface in the basis. If the Fermi surface lies near low Ω values, a smooth energy distribution of the members is predicted, and has been observed for the odd-neutron nucleus ^{99}Ru.[1] If the Fermi surface lies near high-Ω values, as is the case for ^{111}Ag, a regular energy dependence is not expected, and the resultant energy pattern is very sensitive to details

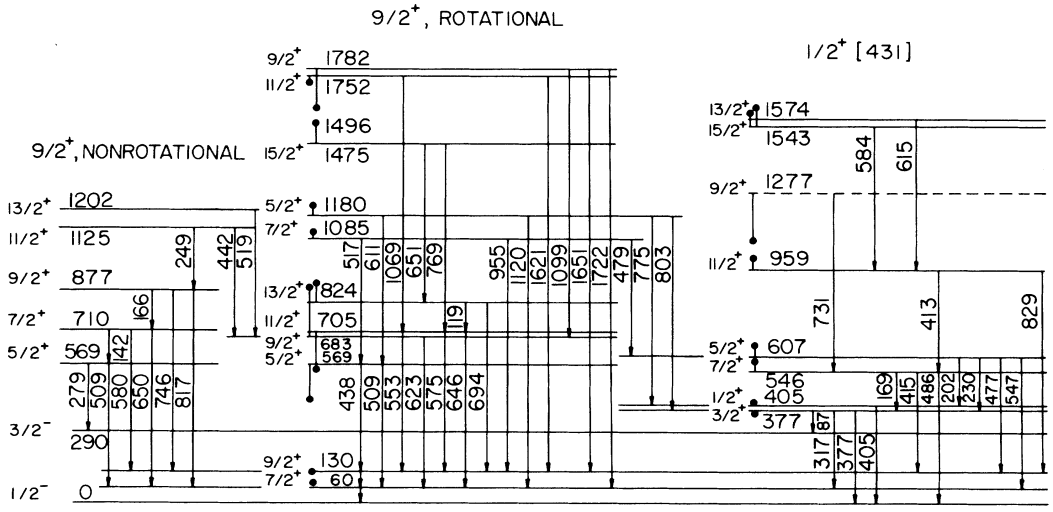

FIG. 6. Interpretation of positive parity states in ^{111}Ag. The right-most group of states has been identified as members of a rotational band. The central group has been identified as members of rotational multiplets. For both groups the dots represent energies calculated by the particle-rotor model. The left-most group of states have been tentatively identified as members of a non-rotational multiplet where the $\frac{9}{2}^+$ particle is coupled to the second 2^+ state of the core.

of the calculation. The calculation does provide a reasonable overall characterization of the experimental energies, and in particular gives a natural explanation of the low-lying $\frac{7}{2}^+$ state which persists in all known odd-A Ag isotopes.

The calculation has been successful in identifying many rotational features of ^{111}Ag. There are other states known experimentally which must involve non-rotational excitations of the core not included in the model. While a serious attempt to provide an interpretation of these non-rotational states would be pure speculation without a more complicated model, certain features warrant comments.

Figure 7 shows the experimentally observed states in ^{111}Ag which we propose to be non-rotational. The low-lying non-rotational states of the ^{110}Pd core are included for comparison. The ^{111}Ag states are organized into different columns on the basis of their parities and decay properties. Experimentally, many of these states decay into only one of the five families of rotational states; the $\frac{9}{2}^+$ "multiplet" structure, or a member of the $\frac{1}{2}^+[431]$, $\frac{1}{2}^-[301]$, $\frac{3}{2}^-[301]$, or $\frac{5}{2}^-[303]$ rotational bands. Each column represents one of these families, and is identified at the bottom of the column. States which decay into more than one family are included in more than one column, with a dashed line connecting them to indicate that the same state is involved. A few states also decay by $E1$ transitions and are marked by asterisks.

The group of low-lying positive parity states which decays only to members of the $\frac{9}{2}^+$ family (or within itself) is of particular interest. There are six such states below 1202 keV, and there is a small energy gap between them and the next similar state at 1388 keV. Of these six states, five have the right spins to be candidates for a "multiplet" representing the coupling of a $\frac{9}{2}^+$ particle to the second 2^+ state of the core. (The spin of the sixth state in this group, the 1160-keV state, is not known, but is $\frac{9}{2}$, $\frac{11}{2}$, or $\frac{13}{2}$. The state could also be a possible candidate for the non-rotational multiplet.) Further, the average energy of the five states is 896 keV, which is comparable to the sum (944 keV) of the energies of the lowest $\frac{9}{2}^+$ states in ^{111}Ag and the second 2^+ state of the core. While this association is speculative, it is highly suggestive, and is shown at the left hand side of Fig. 6. The branching ratios for the decay of members of this non-rotational "multiplet" are quite different than those for the rotational "multiplet," as can be seen in Table III. For example, the $\frac{9}{2}^+$ member of the rotational multiplet has a 90% branch to the lowest $\frac{7}{2}^+$ state and only a 10% branch to the lowest $\frac{9}{2}^+$ state, while the $\frac{9}{2}^+$ member of the non-rotational "multiplet" has only a 32% branch to the lowest $\frac{7}{2}^+$ state and a 48% branch to the lowest $\frac{9}{2}^+$ state. Thus the rotational and non-rotational "multiplets" are quite distinct experimentally.

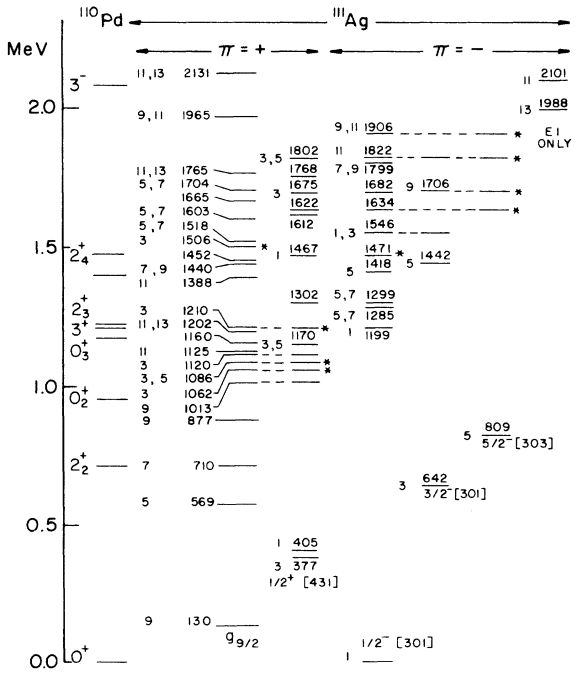

FIG. 7. Non-rotational states in ^{111}Ag, along with non-rotational states of the ^{110}Pd core. Spins of ^{111}Ag states are shown as twice the actual spin. ^{111}Ag states are grouped into columns based on the rotational families to which they decay. An asterisk indicates that the state decays by an $E1$ transition as well.

The distinct branching ratios also means that the wave functions for states in the two "multiplets" are very different. This implies that mixing between rotational and non-rotational states is small. The most dramatic indication of the implied independence of the two degrees of freedom is seen in the $\frac{5}{2}^+$ member of each "multiplet." Not only are the branches of the two states very different, but the two states are essentially degenerate in energy. Since these are the lowest known $\frac{5}{2}^+$ states in ^{111}Ag, it is difficult to imagine that there is any mixing between them at all.

For non-rotational states at higher excitation energies there are too many possible interpretations to indulge in even suggestive speculation. There is, however, an overall trend which is intriguing. The lowest energy non-rotational states in each column increase in energy in a manner that roughly parallels the lowest member of each rotational family to which the non-rotational states decay. Together with the distinct decay properties associated with each column, this suggests that there is experimental information which could help identify the odd-particle parentage of the different non-rotational states. Finally the states which also decay by $E1$ transitions clearly represent some change in structure relative to states below them. We feel that there are enough experimental clues in these data as to the structure involved that a successful interpretation might be feasible if an appropriate calculation were performed.

V. CONCLUSIONS

Use of the proton-γ coincidence system resulted in data far superior to that normally obtained in ^{3}He induced fusion reactions. Not only were photopeaks from compet-

ing reaction channels removed from the spectra, but the reduction in background allowed the placement of many weak transitions in the level scheme. The (^{3}He,pnγ) reaction itself proved to be very effective in populating non-yrast states. The reaction populated all 46 states previously known from β-decay,[4,5] plus 35 new states in the same energy region. Primarily because of the extremely clean spectra reliable spin assignments were made for most of the states from the excitation functions and angular distribution data.

The four rotational bands observed clearly indicate the rotational nature of ^{111}Ag. A basic understanding of these bands, in fact, could have been obtained without a detailed calculation; the bandheads are what one would expect from a Nilsson diagram at a deformation of $\delta \approx 0.2$. In particular the low-lying $\frac{1}{2}^+$ and $\frac{3}{2}^+$ state are a strong signature of the deformation of ^{111}Ag. They are naturally predicted by the Nilsson model as a result of the disappearance of the $Z = 50$ shell closure, but are difficult to explain from a vibrational picture. Our particle-rotor calculation shows that the Coriolis mixing for these bands is small, and has little effect on energies. The proper treatment of the Coriolis interaction is required, however, to explain detailed properties of the bands such as decay properties.

In this rotational nucleus we have also observed a different kind of rotational structure, rotational "multiplets," claimed characteristic of less deformed nuclei such as ^{105}Ag (Ref. 2), ^{99}Ru (Ref. 1), and ^{97}Mo (Ref. 8). We have shown here that these rotational "multiplets" emerge as a result of the larger Coriolis mixing among Nilsson states of $g_{9/2}$ parentage, and are just as natural a prediction of the rotational model as bands.

The detailed agreement between the calculation and experimental results is excellent. The success of this simple model, which assumes axial symmetry, argues that the introduction of an extra degree of freedom by the use of an asymmetric rotor is not necessary for this mass region.

The rotational model satisfactorily accounts for most of the low energy structure of ^{111}Ag. Because of the completeness of the reaction, additional non-rotational states constitute a non-rotational multiplet where the $g_{9/2}$ proton is coupled to the second 2^+ state of the core. Members of this non-rotational multiplet decay in a manner completely different from those in the lowest rotational multiplet, which argues that there is little mixing between the two multiplets. The independence of the underlying degrees of freedom is dramatically indicated by the existence of a state from each multiplet with the same spin and parity at essentially the same excitation energy.

The remainder of the non-rotational state at higher excitation energies exhibit decay patterns which have been used to sort them into families. We feel that these signatures could serve as a focus for calculations similar to those performed for non-rotational states in rare-earth nuclei.[20,21] In principle the interacting boson fermion approximation (IBFA) model[22] can treat both rotational and non-rotational states. However, since at this time the newest IBFA-2 calculation poorly reproduces experimental electromagnetic transition properties,[23] it could not utilize the experimental signatures of the present data.

The present work demonstrates that ^{111}Ag is an important key for the understanding of the collective motion in transitional nuclei. Its deformation is intermediate to the strongly deformed and slightly deformed regions, and its structure exhibits features found in both regions. We believe that the results show that the "multiplets" predicted by our model are just as characteristic of rotational motion in slightly deformed nuclei as are bands in strongly deformed nuclei.

This work was supported in part by the National Science Foundation.

*Present address: 3 Rue said Benkelouas, Constantine, Algeria.
†Present address: Schlumberger Well Services, Houston, Texas 77252.

[1]C.S. Whisnant, K.D.Carnes, R.H. Castain, F.A. Rickey, G.S. Samudra, and P.C. Simms, Phys. Rev. C **34**, 443 (1986).
[2]Sadek Zeghib, F.A. Rickey, and P.C. Simms, Phys. Rev. C **34**, 1451 (1986).
[3]P.C. Simms, F.A. Rickey, and R.K. Popli, Nucl. Phys. **A347**, 205 (1980).
[4]G. Berzins, M.E. Bunker, and J.W. Starner, Nucl. Phys. **A126**, 273 (1969).
[5]W.C. Shick, Jr., and W.L. Talbert, Jr., Nucl. Phys. **A128**, 353 (1969).
[6]R.E. Anderson, J.J. Kraushaar, I.C. Oelrich, R.M. DelVecchio, R.A. Naumann, E.R. Flynn, and C.E. Moss, Phys. Rev. C **15**, 123 (1977).
[7]R.E. Anderson, J.J. Kraushaar, R.A. Emigh, P.A. Batay-Csorba, and H.P. Blok, Nucl. Phys. **A287**, 265 (1977).
[8]K.D. Carnes, F.A. Rickey, G.S Samudra, and P.C. Simms, Phys. Rev. C **35**, 525 (1987).
[9]S.G. Nilsson, K. Dan. Vidensk. Selsk Mat.-Fys. Medd **29**, No. 16 (1955).
[10]R.A. Meyer, Lawrence Livermore Laboratory, Livermore, Calif., Report UCRL M-100 (1978).
[11]R.H. Castain, Ph.D. thesis, Purdue University, 1983.
[12]G. Kajrys, R. LeComte, S. Landsberger, and S. Manaro, Phys. Rev. C **28**, 1504 (1983).
[13]T. Yamazaki, Nucl. Data **A3**, 1 (1967).
[14]B. Harmatz, Nucl. Data Sheets **27**, 453 (1979).
[15]Ch. Vieu, S.E. Larsson, G. Leander, I. Ragnarsson, and J.S. Dionisio, Phys. Rev. C **22**, 853 (1980).
[16]H.A. Smith, Jr. and F.A. Rickey, Phys. Rev. C **14**, 1946 (1976).
[17]Rakesh Popli, J.A. Grau, S.I. Popik, L.E. Samuelson, F.A. Rickey, and P.C Simms, Phys. Rev. C **20**, 1350 (1979).
[18]M.A.J. Mariscotti, G. Scharff-Goldhaber, and B. Buck, Phys. Rev. **178**, 1864 (1969).
[19]B. Reehal and R. Sorenson, Phys. Rev. C **2**, 819 (1970).
[20]D.R. Bes and Cho Yi-chung, Nucl. Phys. **86**, 581 (1966).
[21]V.G. Soloviev and P. Vogel, Nucl. Phys. **A92**, 449 (1967).
[22]C.E. Alonso, J.M. Arias, R. Bijker, and F. Iachello, Phys. Lett. **144B**, 141 (1984).
[23]J.M. Arias, C.E. Alonso, and M. Lozano, Phys. Rev. C **33**, 1482 (1986).